ENVIRONMENTAL RESEARCH
LETTERS

LETTER • OPEN ACCESS

Physical processes driving intensification of future precipitation in the mid- to high latitudes

To cite this article: B Poujol *et al* 2021 *Environ. Res. Lett.* **16** 034051

ENVIRONMENTAL RESEARCH
LETTERS

LETTER

Physical processes driving intensification of future precipitation in the mid- to high latitudes

B Poujol[1], P A Mooney[2] and S P Sobolowski[2]

[1] Département de Géosciences, École Normale Supérieure, PSL. Res. Univ., Paris, France
[2] NORCE Norwegian Research Centre, Bjerknes Centre for Climate Research, Bergen, Norway

E-mail: basile.poujol@ens.fr

Keywords: Norway, precipitation, convection, kilometer-scale modeling, orography

Supplementary material for this article is available online

OPEN ACCESS

RECEIVED
17 September 2020

REVISED
4 January 2021

ACCEPTED FOR PUBLICATION
19 January 2021

PUBLISHED
15 March 2021

Abstract

Precipitation is changing as the climate warms, and downpours can become more intense due to the increased water holding capacity of the atmosphere. However, the exact nature of the precipitation response and its characteristics is still not well understood due to the complex nature of the physical processes underlying the formation of clouds and precipitation. In this study, present and future Norwegian climate is simulated at convection-permitting scales with a regional climate model. The future climate is a high emission scenario at the middle of the century. Hourly precipitation is separated into three categories (convective, stratiform, and orographically enhanced stratiform) using a physically-based algorithm. We investigate changes in the frequency, intensity and duration of precipitation events for each category, delivering a more nuanced insight into the precipitation response to a changing climate. Results show very strong seasonality, with significant intensification of autumn precipitation. An increase in convective precipitation frequency and intensity dominates the climate change signal regardless of season. While changes in winter and summer are well explained by thermodynamical theory, the precipitation response in autumn and spring deviates from the idealised thermodynamic response, partly owing to changes in cloud microphysics. These results show that changes in the precipitation distribution are affected in complex ways by the local climatology, terrain, seasonality and cloud processes. They illustrate the need for further and more detailed investigations about physical processes underlying projected precipitation changes and their seasonal and regional dependence.

1. Introduction

Thanks to rain gauge observations, particularly hourly observations, it is now clear that there has been a significant increase in the intensity of extreme precipitation since the preindustrial period (Min *et al* 2011). There is 'medium confidence' that this is a consequence of increasing temperature due to anthropogenic emissions of greenhouse gases (IPCC 2013). This confirms early model predictions (Manabe and Wetherald 1975). However, observed increases are larger than those predicted by climate models in Europe (Fischer and Knutti 2016) and the Northern Hemisphere (Min *et al* 2011).

This fact is of particular importance since precipitation has major knock-on effects on a range of economic sectors, and can be responsible for damage affecting human life and health, ecosystems, infrastructure and cultural heritage.

Precipitation can arise from a variety of mechanisms and can be classified into types, such as convective, stratiform, and orographic (Houze 1981, Houze 2012). These processes might respond differently to the increase of global temperatures.

A host of different physical mechanisms have been invoked to explain observed changes in precipitation characteristics. Among these are: increases in atmospheric moisture according to the Clausius–Clapeyron relationship and subsequent increased latent heating in precipitating systems (Westra *et al* 2014), transitions from stratiform to convective rainfall (Berg *et al* 2013, Molnar *et al* 2015), diminution

of precipitation area (Loriaux *et al* 2017, Benestad 2018), changes to the eddy-driven jet leading to a reduction of the Rossby deformation radius affecting both position and intensity of mid-latitude disturbances (Dwyer and O'Gorman 2017), vertical shift of the melting level (Prein and Heymsfield 2020). These involve different temporal and spatial scales as well as physical processes, which can, and often are, studied separately.

Nevertheless, these processes are actually coupled. Insofar as a complete theoretical and physical approach of these changes is not possible, models are required to describe the full range of mechanisms. Recent advances in computational power have enabled regional climate models (RCMs) to simulate the climate at convection-permitting resolutions (Prein *et al* 2015). Convection-permitting RCMs remove many uncertainties related to precipitation as convective processes are no longer parameterised. Instead, they are represented by the primitive dynamic and thermodynamic equations (Brisson *et al* 2016). Although it is now known that models permit convection at grid spaces as large as 25 km (Vergara-Temprado *et al* 2020), an improved representation of fundamental precipitation characteristics by kilometer-scale models is acknowledged and has been broadly evaluated and confirmed (Ban *et al* 2014, Fosser *et al* 2017, Kendon *et al* 2017, Berthou *et al* 2018b, Chan *et al* 2018, Keller *et al* 2018, Finney *et al* 2019). More recently, the added value of these models has been demonstrated over Scandinavia by Lind *et al* (2020). However, the use of these models for studying climate change impacts on precipitation is relatively new and little is known about the physical processes driving these changes.

Early studies (Kendon *et al* 2014) showed that these convection-permitting models are able to reproduce the expected strong increase in precipitation intensity with global warming, and this response is strongly dependent on location and season. However, most existing convection-permitting modeling studies are limited to a description of the output. We believe that these models can also help us understand the physical processes responsible for the observed and simulated changes, since these processes are explicitly present in the model output.

This work aims to elucidate the changing characteristics of precipitation in order to better understand the dominant processes that drive the response in middle and high latitudes, with Norway as an example. The letter is structured as follows: section 2 describes the model data, and section 3 presents the methodological techniques. Section 4 briefly describes the physical theory underpinning the precipitation response to warming. Results are presented in section 5 and discussed in section 6, where we also examine physical processes that elucidate the results.

2. Materials and methods

2.1. Model setup

We use the Advanced Weather Research and Forecasting (WRF) model version 3.9.1.1 (Skamarock *et al* 2005) with 3 km grid spacing. The model uses 1-way nesting, i.e. the boundary conditions are first given to an intermediate simulation at 15 km resolution (in which convection is parameterised), running over Europe, and then this simulation gives boundary conditions to the final simulation at 3 km resolution over Scandinavia. In the 3 km domain, the convective parameterisation is switched off and all precipitation is produced by the microphysical scheme, described in Thompson *et al* (2008). Other parameterisations include the RRTMG radiation scheme (Iacono *et al* 2008), the Yonsei University planetary boundary layer scheme (Hong *et al* 2006), the revised Monin-Obukhov surface layer scheme (Jiménez *et al* 2012), and the Noah multi-physics land surface model (Noah-MP; (Niu *et al* 2011)). Please see Mooney *et al* (2021) for further details about the model configuration and evaluation.

2.2. Surrogate warming experiment

Two simulations are conducted. In a control simulation, the European Centre for Medium Range Weather Forecasting Interim Reanalysis (ERA-Interim, (Dee *et al* 2011)) provides boundary conditions including sea surface temperatures (SST) during the period 1996–2005. The second simulation is a surrogate warming experiment (Schär *et al* 1996) under the RCP8.5 scenario at the middle of the century which corresponds to approximately 1.5 °C of warming globally. Boundary conditions are still given by the ERA-Interim dataset of 1996–2005, but they are perturbed by adding a monthly change that corresponds to the difference in the monthly mean of temperature, moisture, wind, geopotential height and SST in the CMIP5 (Coupled Model Intercomparison Project) simulations listed in appendix D between the periods 1976–2005 and 2035–2065. The experimental setup implies that only weak large-scale dynamical changes are present in the data, thus the precipitation changes will be due mainly to thermodynamical and microphysical processes. We also note that while the moisture is perturbed at the lateral boundaries, within the domain all aspects of the water cycle are allowed to occur freely. Domain-mean temperature and precipitation increases between the control and surrogate warming simulations are 2.1 °C (2.3 °C over land only) and 82 mm yr^{-1} (120 mm yr^{-1} over land only).

2.3. Analysis of the rain rate distribution

We analyse the full distribution of precipitation rates using the Analyzing Scales of Precipitation (ASoP,

(Klingaman *et al* 2017)) technique. For a detailed description of the technique, the reader is referred to Berthou *et al* (2018b) (see their figure 2 for a summary). This method has become widely used in the convection-permitting modeling community (Berthou *et al* 2018b, Kendon *et al* 2019, Lind *et al* 2020, Vergara-Temprado *et al* 2020), because it enables a comprehensive view of precipitation changes across the whole distribution of precipitation rates, from drizzle to heavy downpours. A histogram of precipitation rates is calculated, providing a frequency of occurrence f_i for each bin ($1 \leqslant i \leqslant n$). This frequency can be multiplied by the value of the bin centre b_i to obtain the *actual* contribution of this bin to total precipitation $f_i b_i$. This actual contribution is then averaged over all the grid points of the sub-region of interest. The mean precipitation rate is then $P = \sum_{i=0}^{n} f_i b_i$ and the *fractional* contribution from each bin to total precipitation is $f_i b_i / P$. The actual contribution changes show the changes in the amount of precipitation produced by each precipitation rate, whereas the fractional changes show the changes in the shape of the distribution only.

2.4. Uncertainty quantification

For uncertainty quantification, a bootstrapping technique by yearly blocks is used (Hesterberg 2015): 10 000 random data samples are produced by choosing with replacement 10 random years within the 10 years of both the control and the future simulations. Each sample provides a curve/histogram and future-present differences and, depending on the confidence level, appropriate percentiles of these histograms are taken as the limits of the uncertainty interval.

2.5. Classification of precipitation

Precipitation is separated into different categories in order to provide a better physical understanding of how precipitation changes in a warming climate. Three precipitation types are considered: convective, stratiform and orographically enhanced stratiform precipitation (hereafter orographic). Because there are no convective parameterisations in convection-permitting models, precipitation is not classified in the model output as it is in state-of-the-art regional climate models. A separation algorithm is needed. We use a physically-based algorithm that is suited for mountainous areas. It is based on three dimensional wind speed. Convection is detected via identification of its overturning circulation and its horizontal potential vorticity dipoles. The description of the algorithm, as well as precise definitions of the three categories of precipitation, can be found in Poujol *et al* (2020). This reference also contains an evaluation and validation of the algorithm with various datasets and time scales ranging from the hourly to the climatological.

3. Region of interest

The domain covers most of Scandinavia, however, this analysis only focuses on Norway (figure 1(a)). The country presents strong climatic contrasts. Southern Norway is separated into east and west by the Scandes, a wide mountain ridge with peaks above 2000 m. The western region (Vestlandet) is strongly influenced by the North Atlantic storm track, with precipitation from land-falling storms and frontal systems often enhanced by uplift over the Scandes, leading to annual precipitation amounts of 1500–6000 mm, peaking in winter. In contrast the Eastern part of the mountains (Østlandet) is a more continental climate, with stratiform precipitation coming from the South and the South East peaking in fall, and predominantly convective precipitation in summer. Annual precipitation in the eastern part is 500–1000 mm. Moving north, the mountains are lower and the climate transitions from a mid-latitude climate towards a sub-Arctic climate in Hålogaland with precipitation amounts of 1000 to 2500 mm. In this study, Norway is separated into five sub-regions, that are defined by merging precipitation regions defined in Hanssen-Bauer *et al* (2009). As shown in figures 1(b) and (c), the simulated annual precipitation compares favourably with the seNorge2018 gridded observational product. Also plotted on figure 1(c) is the stations that underlie the seNorge2018 product, which is produced on a 1 km grid and covers the period from 1957 to present (Lussana *et al* 2019). WRF underestimates the contrasts of precipitation in Norway, with an underestimation of precipitation on the West coast and a slight overestimation in the East. However, gauge based-gridded precipitation datasets are suspect in mountainous regions (Lundquist *et al* 2019), partly due to poor station density (figure 1(c)). For a more thorough evaluation of the model please refer to Mooney *et al* (2021). The remainder of this paper only considers the precipitation increases shown in figure 1(d) for Western Norway (Vestlandet), Eastern Norway (Østlandet) and Northern Norway (Hålogaland). Results for Trøndelag and Sørlandet are available in the supplement (available online at stacks.iop.org/ERL/16/034051/mmedia).

4. Theoretical background

Basic physical laws and a simple representation of a cloud show that the precipitation rate is roughly the product of three terms (see appendix B for calculations):

- The moisture content at the surface (q_{sat}). This increases with temperature at a rate of 7% per degree of warming in agreement with the Clausius–Clapeyron equation (Clausius 1850);

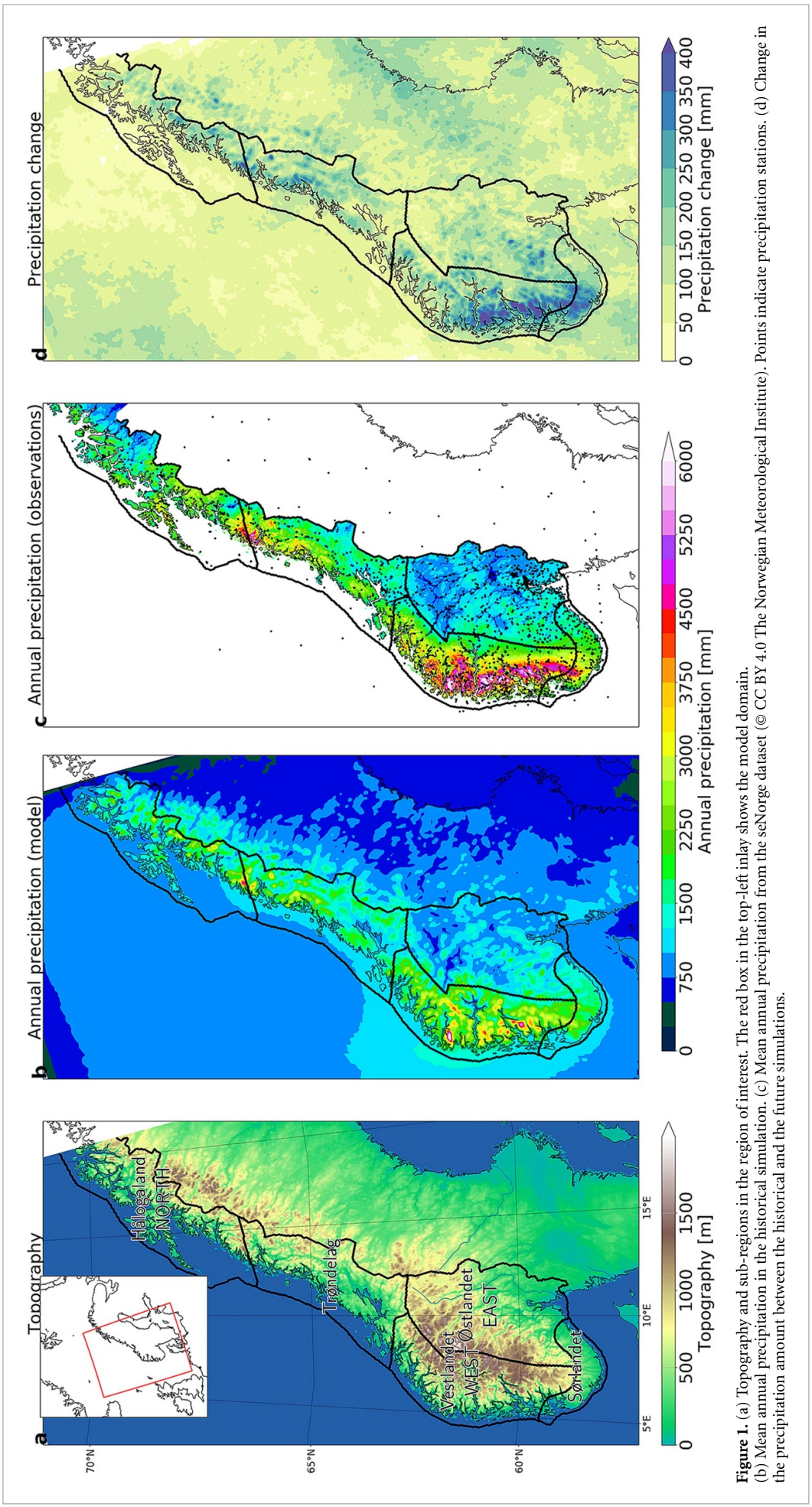

Figure 1. (a) Topography and sub-regions in the region of interest. The red box in the top-left inlay shows the model domain. (b) Mean annual precipitation in the historical simulation. (c) Mean annual precipitation from the seNorge dataset (© CC BY 4.0 The Norwegian Meteorological Institute). Points indicate precipitation stations. (d) Change in the precipitation amount between the historical and the future simulations.

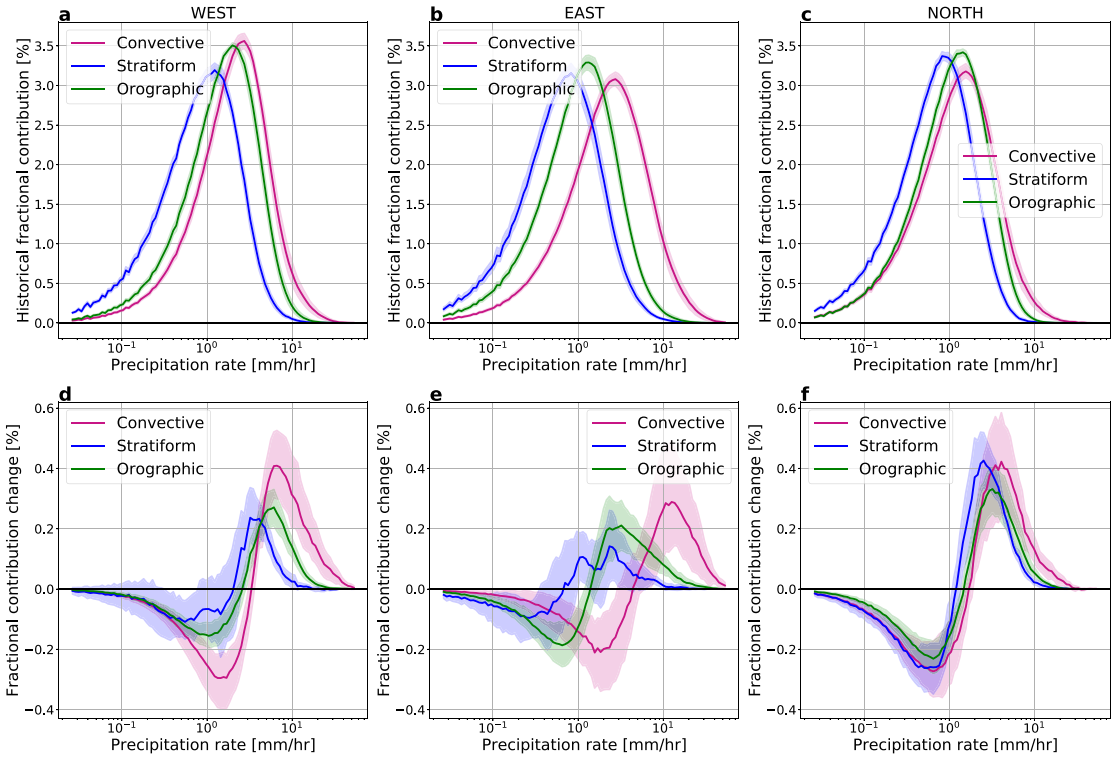

Figure 2. (a)–(c) Fractional contributions of each precipitation rate to total precipitation, for different sub-regions (see panel titles) and different precipitation types as indicated in the legend. (d)–(f) Changes in the fractional contribution (PGW-control). Shading indicates bootstrap uncertainty bounds at the 95% level.

- The vertical velocity in the cloud (w) that depends mainly on water condensation in the cloud;
- The precipitation efficiency (ε) which represents the efficiency of cloud microphysical processes to convert condensed water into rain drops or snow flakes large enough to precipitate. It varies from 0 (totally inefficient) to 1 (100% efficient).

Whereas increasing water vapor always corresponds to an intensification of precipitation under atmospheric warming, the other two factors can increase or decrease.

5. Results

Figure 2 depicts the changes in the fractional contributions of each precipitation rate to the total precipitation (defined in section 2.3). For all precipitation types, the relative contribution of heavy precipitation increases at the expense of the contribution of lower precipitation rates, leading to an overall intensification. The strongest intensification is found for convective precipitation, with the strongest(weakest) shift found in Eastern(Northern) Norway.

The distributions of the intensity and the duration of precipitation events, as well as their modeled changes, are presented in figure 3. A precipitation event is defined, on a given grid point, as a consecutive sequence of precipitation rates exceeding 0.1 mm hr^{-1}. Its peak intensity is the maximal hourly rain rate that is attained during the event. Note that because of this Eulerian approach, the number of grid points and the duration of events associated with a moving precipitating system will depend on its speed. Changes in the distribution are strongly dependent on precipitation type. Convective precipitation becomes more frequent across the entire distribution (figures 3(a)–(c)), and changes are larger in the tail, for the most intense and longest events. This might indicate an increased frequency of organized convection and orographically enhanced convection lasting for several hours. Conversely, the distribution of orographically enhanced stratiform precipitation exhibits a pronounced shift towards higher peak intensities in a future climate. The frequency of events with a peak intensity above 10 mm hr^{-1} more than doubles. Stratiform precipitation is less affected. However, one can see an extension of this distribution towards short and intense events (which might be an artifact due to the misclassification of shallow convection as stratiform precipitation as noted in Poujol *et al* (2020)).

The changes in the actual contributions of each precipitation rate to total precipitation are depicted in figure 4. Unlike fractional contributions, the changes in actual contributions provide information on the change in the amount of each precipitation type, which is the area under the curve. A comprehensive view of changes in the frequency, intensity and distribution of precipitation can be reached only if figures 3

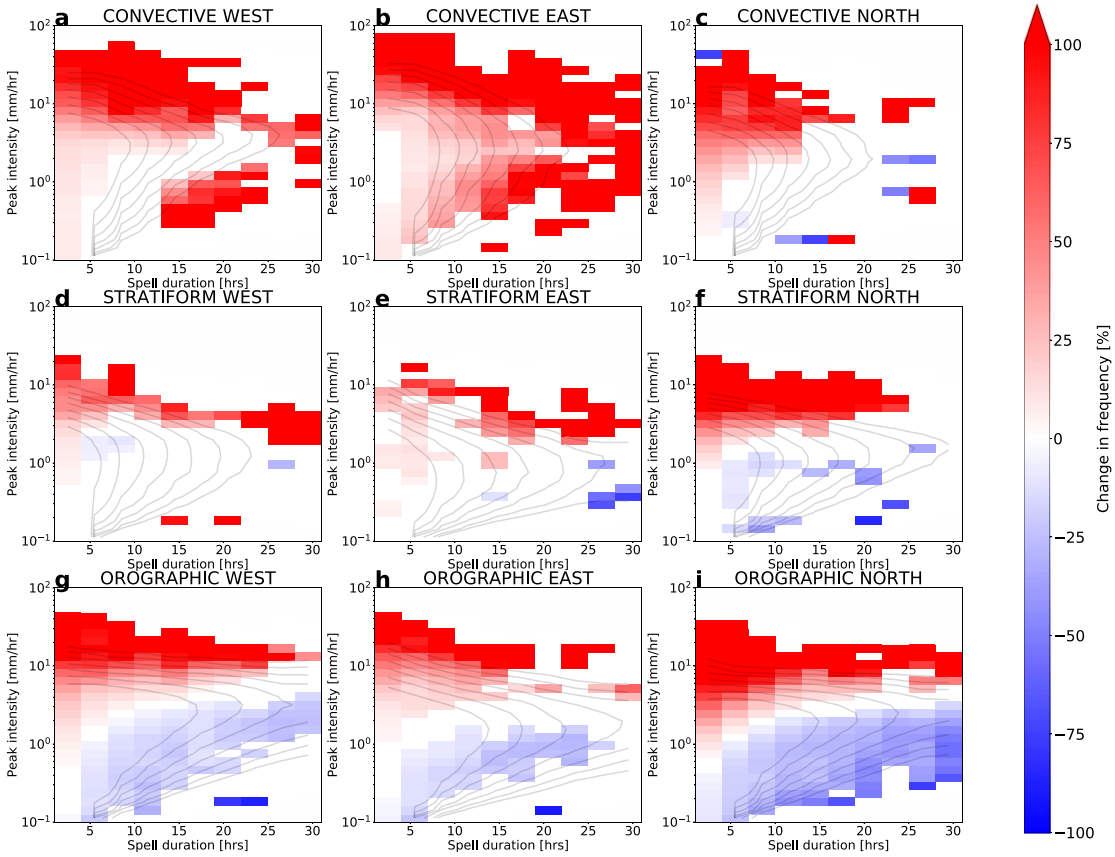

Figure 3. Contours: joint distribution of the peak intensity and the duration of precipitation events. Shading shows the relative change in the distribution between the historical and the future simulation. Non significant changes are masked out. Rows and columns correspond to different precipitation types and sub-regions, as indicated in the panel titles: (a)–(c) convective precipitation; (d)–(f) stratiform precipitation; (g)–(i) orographic precipitation. Contours are logarithmic, their value are 1000, 2000, …, 64 000 mm^{-1}.

and 4 are considered together. In the interest of brevity we summarise the key points arising from such a examination:

- All precipitation types exhibit increased amounts and intensities in autumn, mostly coming from moderate to heavy rainfall (brown curves on figure 4). Figures 3(a)–(c) shows that the main contribution comes from an increase in both the frequency and the intensity of convective precipitation, even for long duration events, although intense orographic precipitation also has a significant contribution (figures 3(g)–(i)).
- Convective precipitation exhibits the strongest response to global warming. Both frequency (figures 3(a)–(c)) and intensity (figures 2(d)–(f)) increase across all seasons. Further, all precipitation rates contribute to the increase, except summer in the East where low and moderate rates decrease (figures 4(a)–(c)). Intensification of convection is strongest in summer and autumn, and weakest in spring (figures 4(a)–(c)).
- Orographic precipitation exhibits little change in overall frequency (figures 3(g)–(i)) but moderate and heavy precipitation become more frequent at the expense of light precipitation (figures 2(d)–(f) and 3(g)–(i)). Contribution from rates over 1 $mm\,hr^{-1}$ is increased, except summer in the East (figures 4(g)–(i)). A pronounced intensification is found (figures 3(g)–(i)), mainly in winter and autumn (figures 4(g) and (h)). In Northern Norway the intensification is found all year round (figure 4(i)).
- Stratiform precipitation exhibits weak changes that are generally insignificant(figures 3(d)–(f) and 4(d)–(f)), except in spring where all precipitation rates contribute to a statistically significant increase (figures 4(d) and (e)).

6. Discussion

In this section, we explore the consistency of our results season by season with other studies. We also provide some insight to the physical processes that could explain these results.

6.1. Winter

The winter changes correspond relatively well to the expected theoretical response of precipitation (section 4). The increase in orographic precipitation comes mainly from the contribution from the high

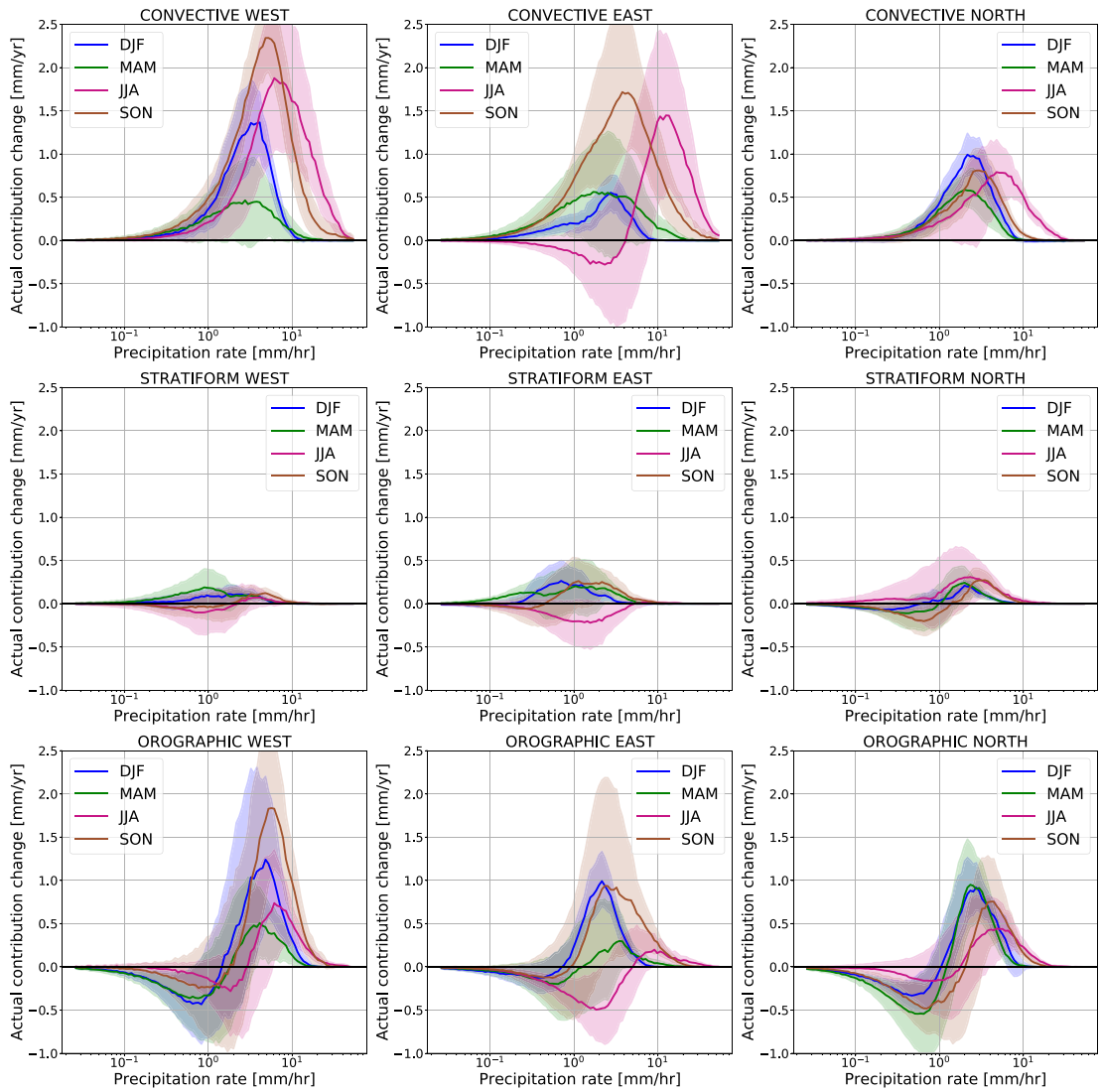

Figure 4. Changes in the actual contributions of each precipitation rate to total precipitation, for different sub-regions (different columns), different precipitation types (rows) and different seasons as indicated in the legend. Shading indicates bootstrap uncertainty bounds at the 95% level. The reference distributions from the historical simulation are available in appendix E.

rates. The constant relative humidity assumption is almost satisfied (figure 5).

A significant increase in convective precipitation intensity and amount is found, and this is consistent with the observations reported by Rulfová and Kyselý (2013), who show that the convective activity is related to surface temperature. This was also found by Gentine *et al* (2013) in a theoretical one-dimensional boundary layer model, where a high surface temperature clearly helped the onset of convection. Recently, Kendon *et al* (2020) also found an increased frequency of wintertime convection over the United Kingdom of Great Britain and Northern Ireland, attributable to an increased sea surface temperature and more convective systems advected onshore from the sea. This is consistent with figure 4 that shows significant increases in wintertime convective precipitation in coastal regions (North and West).

6.2. Summer in Eastern Norway

In Eastern Norway in summer, a decrease in the the frequency of low and moderate precipitation rates is found, and only the highest precipitation rates (over 10 mm hr^{-1}) contribute to increasing amounts of convective and orographic precipitation. This is similar to summer results in other mid-latitude continental regions, such as the central United States (Liu *et al* 2017), or Southern Europe (Berthou *et al* 2018a) where a strong drying is found in summer. Dai *et al* (2017) propose the following mechanism: global warming leads to increased surface atmospheric stability because of the decreasing moist adiabatic lapse rate, and thus more convective inhibition (CIN). Convective available potential energy (CAPE) can therefore accumulate over a stable surface layer. Only precipitation events with the strongest forcing can then be initiated. They have a higher intensity because they can retrieve more CAPE from

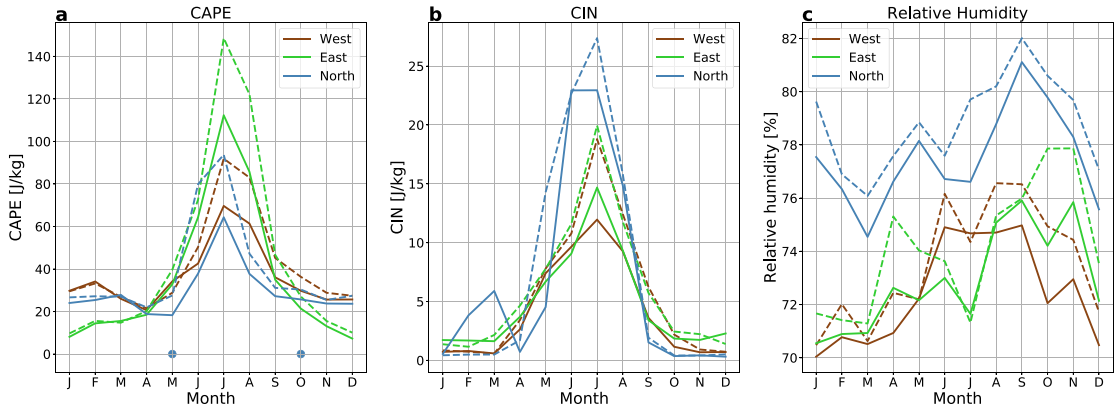

Figure 5. Annual cycle of different variables in the control (solid lines) and surrogate warming (dashed lines) simulations. Colours correspond to different subregions as indicated in the legend. A colored dot on the *x*-axis indicates that the solid and dashed curves of the color of the dot are significantly different at a 95% confidence level. Abbreviations correspond to the following: CAPE = convective available potential energy; CIN = convective inhibition.

the upper troposphere, and remove more moisture from the boundary layer. Thus, moisture takes more time to recover by surface evaporation, which implies decreasing precipitation frequency.

This theory is in good agreement with our simulations, which exhibit an increase in CAPE and CIN, however, these are not statistically significant (figure 5).

6.3. Autumn and summer

The strongest responses are found in autumn (as well as summer in Western and Northern Norway) with dramatic increases in precipitation amounts. Strong increases in midlatitude autumn precipitation amounts have also been found in other studies, e.g. de Luis *et al* (2010) in Spain, Berthou *et al* (2018a) in Southern and Western Europe, and Liu *et al* (2017) in summer and autumn over the Rocky mountains. Berthou *et al* (2018a) also found a shift in the seasonality of extreme precipitation from summertime to autumn in Western, Southern and Central Europe. By separating precipitation in this study, a more thorough comprehension of the mechanisms responsible for autumn changes can be reached.

Our results show a very strong increase in convective precipitation frequency and intensity, as well as an increase in orographic precipitation intensity (figure 3). Substantial changes (over a doubling) are simulated for long-lasting, intense convective events (figure 3), and these occur mainly in summer and autumn (not shown). These more frequent long-lasting convection events are probably associated with orographically-sustained convection (i.e. convection fed by the uplift of a moist air layer over a mountain ridge), that can persist for several hours at the same place in opposition to isolated convective events that are usually short-lived. This would be consistent with the results of Cannon *et al* (2012).

An increase of relative humidity is also evident (figure 5). This might partly explain why such a strong intensification of precipitation occurs in autumn.

6.4. Spring

Spring exhibits weak responses in precipitation intensity and frequency. However, a significant increase in the amount of stratiform precipitation is found. To the best of our knowledge, such a result has not been noticed previously in the literature. This change cannot be explained by dynamical changes such as a latitudinal shift of the storm tracks, because the surrogate warming framework conserves weather (geopotential changes are only used to avoid breaking of the thermal wind relation). A possible reason would be that more rain than snow occurs in warmer conditions. Because the fall speed of rain is faster, it has less time to evaporate, and so precipitation would be more likely to reach the ground. However, we note that this result could also be due to more frequent shallow convection that is misclassified as stratiform precipitation because convection is not deep enough (this is a known shortcoming of the classification algorithm (Poujol *et al* 2020)).

6.5. Microphysical explanations

Basic thermodynamic considerations fail to fully explain the seasonality of the precipitation response. Since large-scale dynamical changes are almost not taken into account in these simulations, this suggests that changes in the precipitation characteristics are likely due to microphysical processes. Such microphysical changes have already been noticed by Singh and O'Gorman (2014). To investigate these changes we make an estimation of the precipitation efficiency, which represents the efficiency of the conversion of water sources into precipitation by cloud processes. This estimation is presented in appendix C. When

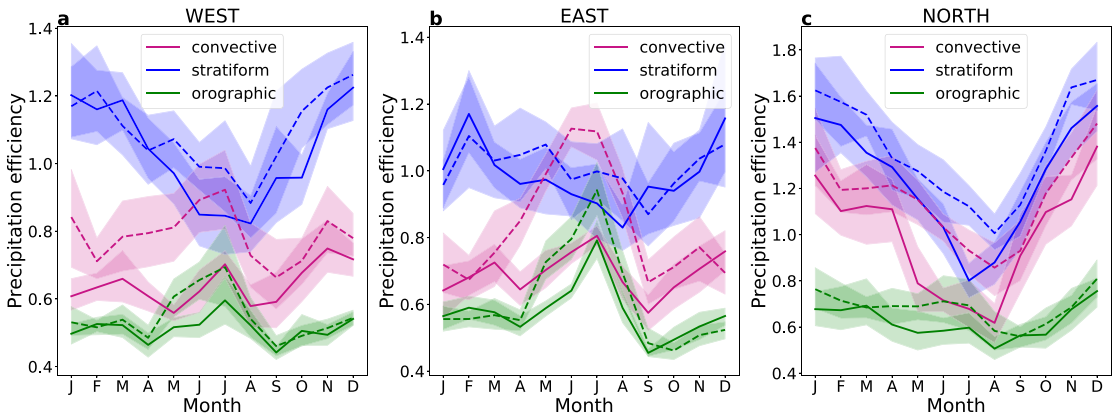

Figure 6. Annual cycle of precipitation efficiency for different precipitation types as indicated in the legend. Solid lines: control simulation. Dashed lines: surrogate warming simulation. Different panels correspond to different subregions as indicated in the panel titles. Shadings show an uncertainty interval with 95% confidence using bootstrapping by yearly blocks.

looking at the results, presented in figure 6, several points emerge:

- Stratiform precipitation is by far the most efficient. It is formed by supersaturated water vapor deposition on the snow flakes, which then fall. The mechanism is supposed to be almost 100% efficient (Findeisen 1938, Cannon *et al* 2012). Stratiform precipitation shows the highest efficiency in winter, when temperatures are colder and when the condensation of vapor on snow flakes occurs more frequently.
- Orographic precipitation is not efficient. An explanation is that when moist air is forced to ascend over mountains, water vapor condenses close to the ground. Clouds are therefore mostly liquid, and the precipitation is very inefficient (Findeisen 1938) because most of the water condensate stays in the water column and does not precipitate.
- Precipitation efficiency for stratiform and orographic changes little in a future warmer climate. However, the efficiency of convective precipitation increases considerably. This increase is concentrated during the warm season when temperatures are above freezing in the lower troposphere (from late spring to early autumn in Northern and Eastern Norway where the warm season is short, but almost all year round in western Norway where winters are milder). As suggested by Prein and Heymsfield (2020), increases in the freezing level height can lead to more efficient riming in deep convective clouds, leading to more intense precipitation.

These changes in cloud microphysics and in precipitation efficiency shed some light on the mechanisms responsible for the strong response of convective precipitation in summer and autumn. Indeed, the intensity of convective precipitation increases well above the Clausius–Clapeyron rate (not shown), likely owing in part to these processes.

7. Conclusions

Precipitation is changing in a warming climate and has major impacts on human activities. This study investigated the physical processes driving the response of hourly precipitation to climate change through the use of convection-permitting climate simulations of the current and future climate (represented by the surrogate warming experiment). Results are consistent with previous work, and exhibit an increase in precipitation amounts in a future climate, mainly due to an increase in event intensity rather than frequency. This study brings new knowledge insofar as it delves into the separation of precipitation types. The precipitation response strongly depends on both seasonality and precipitation type, with convective precipitation being the most sensitive to warming. Whereas the response of precipitation intensity during winter and summer is well explained by thermodynamical theory, more complex changes occur during the transition seasons. These changes result from an interplay between various thermodynamic and microphysical mechanisms. In particular, a dramatic increase in autumn rainfall is found which likely results from the interaction between increased relative humidity and an increase of convective precipitation efficiency. While the evidence presented here suggests super Clausius–Clapeyron scaling (Lenderink *et al* 2017), particularly in summer-autumn, the theory relies on a complex interplay of processes. Further work that focuses on these is needed before a robust conclusion can be determined.

Due to the prohibitive computational costs of running multiple simulations, this study relies on a single model which limits the reliability of our results. An ensemble of convection-permitting simulations

would be preferable to assess model uncertainty, and support or contradict our results. One promising initiative is the World Climate Research Program Coordinated Regional Downscaling Experiment Flagship Pilot Studies (WCRP-CORDEX-FPS) (Coppola *et al* 2019) which benefits from the coordination and combined computational resources of multiple institutions. Perhaps one of the most important issues raised by this work is the striking difference between precipitation response in spring and in autumn. Changes are very weak in spring, whereas a large intensification was found in autumn, consistent with many other studies. This likely indicates that there is some fundamental thermodynamic or microphysical reason for this autumn precipitation increase, but this reason has not been elucidated yet. Future work could extend the physical analysis by using idealised models to investigate responses during the transition seasons.

Data availability statement

The data that support the findings of this study are available upon reasonable request from the authors.

Acknowledgment

B P warmly thanks Nicolas Rochetin for evaluating and giving feedback on an internship report from which this letter is largely inspired. Analysis was performed on resources provided by UNINETT Sigma2—the National Infrastructure for High-Performance Computing and Data Storage in Norway (NN9280K, NN9468K, NS9599K). The authors gratefully acknowledge support from the Research Council of Norway (Grant No. 268243) and its basic institute support of their strategic project on Climate Services.

Appendix A. Mathematical notations

T	Temperature	K
p	Pressure	Pa
z	Altitude	m
ρ	Density	$\mathrm{kg \cdot m^{-3}}$
$\vec{u} = u\vec{i} + v\vec{j} + w\vec{k}$	Wind velocity	$\mathrm{m\ s^{-1}}$
q_v	Mixing ratio of water vapor	No unit
q_{CL}	Mixing ratio of cloud water	No unit
q_{sat}	Saturated mixing ratio of water vapor	No unit
e_s	Saturated water vapor partial pressure	Pa
$RH = q_v/q_{\mathrm{sat}}$	Relative humidity	%
$C = -\mathrm{d}q_{\mathrm{sat}}/\mathrm{d}t$	Condensation	$\mathrm{s^{-1}}$
P	Precipitation	$\mathrm{mm \cdot hr^{-1}}$
E	Evaporation	$\mathrm{mm \cdot hr^{-1}}$
ε	Precipitation efficiency	No unit
p_0	Reference pressure	1000 hPa
R	Specific gas constant of dry air	$284\ \mathrm{J \cdot K^{-1} \cdot kg^{-1}}$
R_v	Specific gas constant of water vapor	$461\ \mathrm{J \cdot K^{-1} \cdot kg^{-1}}$
c_p	Specific heat capacity of water at constant pressure	$1004\ \mathrm{J \cdot K^{-1} \cdot kg^{-1}}$
L_v	Specific latent heat of vaporisation of water	$2500\ \mathrm{J \cdot kg^{-1}}$

Appendix B. Theoretical expectations

Let us consider an air particle moving upward from the surface, eventually producing precipitation through adiabatic lifting. According to the Clausius–Clapeyron relation (Clausius 1850), the water holding capacity of the parcel increases almost exponentially with temperature (approximately 7% per degree of warming):

$$\frac{1}{e_s}\frac{\mathrm{d}e_s}{\mathrm{d}T} = \frac{L_v}{R_v T^2} \tag{B1}$$

(All mathematical notations are defined in appendix A.) Moreover, precipitation P is the vertical integral of condensation C in the air column multiplied by a precipitation efficiency ε (equality 2.a):

$$P \underset{(a)}{=} \int_{z=0}^{\infty} \epsilon C \rho \mathrm{d}z \underset{(b)}{=} -\int_0^{\infty} \epsilon \frac{\mathrm{d}^* q_{\mathrm{sat}}}{\mathrm{d}^* t} \rho \mathrm{d}z$$
$$\underset{(c)}{=} -\int_0^{\infty} \epsilon w \rho \frac{\partial q_{\mathrm{sat}}}{\partial z}\mathrm{d}z \underset{(d)}{\approx} -\epsilon w \rho_0 \int_0^{\infty} \frac{\partial q_{\mathrm{sat}}}{\partial z}\mathrm{d}z$$
$$\underset{(e)}{=} \epsilon w \rho_0 q_v(z=0) \tag{B2}$$

where d* represents a Lagrangian derivative along a moist adiabat. Since q_{sat} depends only on temperature, and temperature can change only by vertical motion (in an adiabatic movement), it can be transformed into a vertical derivative (equality 2.c). Then, precipitation efficiency, air density and vertical velocity are assumed to vary slowly in the vertical compared to moisture, and are therefore taken out of the integral, following Muller *et al* (2011) (approximation 2.d). The result is that the surface precipitation intensity change is the sum of a thermodynamic term, a dynamical term and a microphysical term:

$$\frac{\delta P}{P} \approx \frac{\delta q_v(z=0)}{q_v(z=0)} + \frac{\delta w}{w} + \frac{\delta \epsilon}{\epsilon} \tag{B3}$$

Whereas the first term always corresponds to an intensification, the two other ones can be either positive or negative depending on situations.

Appendix C. Precipitation efficiency definition

There are many different ways of defining the precipitation efficiency. This quantity is supposed to represent the efficiency of the thermodynamical and microphysical processes that convert water supply into precipitation. To estimate it, different definitions have been suggested. In this study, we revisit one of the two definitions provided by Sui *et al* (2007). Their first definition corresponds to a microphysical precipitation efficiency, traducing the efficiency of the conversion of condensate into precipitation. This definition, the most common one, was used in section 4 of the main text presenting the theoretical response of precipitation to warming. We focus here on the second one, which is a large scale precipitation efficiency and represents the efficiency of conversion of water (vapor or condensate) into precipitation. This second definition is the following:

$$\epsilon = \frac{P}{\sum_{i=1}^{4} \mathrm{sgn}(Q_i) Q_i} \tag{C1}$$

where sgn is the Heaviside function ($\mathrm{sgn}(x) = 1$ if $x > 0$ and 0 otherwise), and $\vec{Q}$ is the vector containing four source terms of water content (liquid, solid and vapor) in an air column:

$$\vec{Q} = \left(\underbrace{-\frac{\partial[q_v]}{\partial t}}_{(1)} ; \underbrace{-[\vec{\nabla}\cdot(\vec{u}q_v)]}_{(2)} ; \underbrace{E}_{(3)} ; \underbrace{-\frac{\partial[q_{CL}]}{\partial t} - [\vec{\nabla}\cdot(\vec{u}q_{CL})]}_{(4)} \right) \tag{C2}$$

where $[\cdot]$ denotes a vertical integration over the troposphere depth, q_v is the water vapor mixing ratio, E is the evaporation, $\vec{u}$ is the wind, and C is the cloud water mixing ratio. The four terms account respectively for (1) the local loss of water vapor in the air column, (2) the advection and convergence of water vapor into the air column, (3) the surface evaporation, and (4) the advection, convergence of cloud water and its local loss. Each of these terms can contribute to the precipitation if, and only if, it is positive. This is why they are multiplied by a Heaviside function.

It is possible to decompose the second term: $-[\vec{\nabla}\cdot(\vec{u}q_v)] = -[(\vec{\nabla}\cdot\vec{u})q_v] - [\vec{u}\cdot\vec{\nabla}q_v]$. We argue that in most of the cases, the advection of water vapor by the wind $-[\vec{u}\cdot\vec{\nabla}q_v]$ is roughly balanced with the local time derivative of precipitable water $-\frac{\partial[q_v]}{\partial t}$, since precipitable water has generally very strong values compared to condensed water. Thus, one of these two terms is generally highly positive and the other one is highly negative (approximately the opposite), and that leads to a strong underestimation of the precipitation efficiency. In this study, we thus gather these two terms in order to consider the contribution of the residual only, which is the Lagrangian time derivative of the column precipitable water. The remaining term, the convergence of moisture into the air column, is kept separated.

Moreover, the cloud water and the water vapor are taken together into these two terms to make the expression simpler.

Because of the limited data of the simulation, the water vapour and cloud water contents that we use are vertically integrated, i.e. the wind is considered to vary slowly in the vertical compared to the atmospheric water content in the integral. This is compatible with the precedent definition only if the wind profile is uniform, which is what we supposed. We thus used the wind at 700 hPa to calculate the Lagrangian derivative and the convergence, assuming most of the water is concentrated in the lower troposphere. Results obtained using a higher level (500 hPa) were similar.

The definition of precipitation efficiency used in this study is thus:

$$\epsilon = \frac{P}{\sum_{i=1}^{3} \mathrm{sgn}(Q_i) Q_i} \tag{C3}$$

where:

$$\vec{Q} = \left(-\frac{\mathrm{D}[q_v + q_{CL}]}{\mathrm{D}t} ; -(\vec{\nabla}\cdot\vec{u}_{700\ \mathrm{hPa}})[q_v + q_{CL}] ; E \right) \tag{C4}$$

and $\mathrm{D}/\mathrm{D}t = \partial/\partial t + \vec{u}_{700\ \mathrm{hPa}}\cdot\vec{\nabla}$ is the Lagrangian derivative computed with the mid-tropospheric horizontal wind $\vec{u}_{700\ \mathrm{hPa}}$. Because of these approximations, the precipitation efficiency can exceed the value of 1. The main errors might occur for disorganized convection, where the moisture of the cells is provided by low-level convergence, which is not well accounted for here because of the wind taken constant at its 700 hPa value. Errors might also come from the fact the the cloud data is only 6 hourly, which is clearly long compared to the time scale of convective precipitation and some orographic precipitation. To avoid large deviations in the mean because of the extreme values that ε can reach, the precipitation efficiencies exceeding 10 have been considered as missing data.

Appendix D. Surrogate warming CMIP5 GCMs

Table D1. CMIP5 GCMs used for deriving the climate perturbations for the surrogate warming simulation.

Model name	Member realisations
ACCESS1-3	r1i1p1
CanESM2	r1i1p1, r2i1p1, r3i1p1
CCSM4	r1i1p1, r2i1p1, r6i1p1
CESM1-CAM5	r1i1p1, r2i1p1, r3i1p1
CMCC-CM	r1i1p1
CNRM-CM5	r2i1p1 r4i1p1, r6i1p1
CSIRO-Mk3-6-0	r1i1p1, r2i1p1,r3i1p1
GFDL-CM3	r1i1p1
GFDL-ESM2M	r1i1p1
GISS-E2-H	r1i1p1, r2i1p1
HadGEM2-CC	r1i1p1, r2i1p1, r3i1p1
HadGEM2-ES	r3i1p1
INM-CM4	r1i1p1
IPSL-CM5A-MR	r1i1p1
MIROC5	r1i1p1, r2i1p1, r3i1p1
MIROC-ESM	r1i1p1
MPI-ESM-LR	r1i1p1, r2i1p1, r3i1p1
MPI-ESM-MR	r1i1p1
MRI-CGCM3	r1i1p1

Appendix E. Precipitation distribution in the control simulation

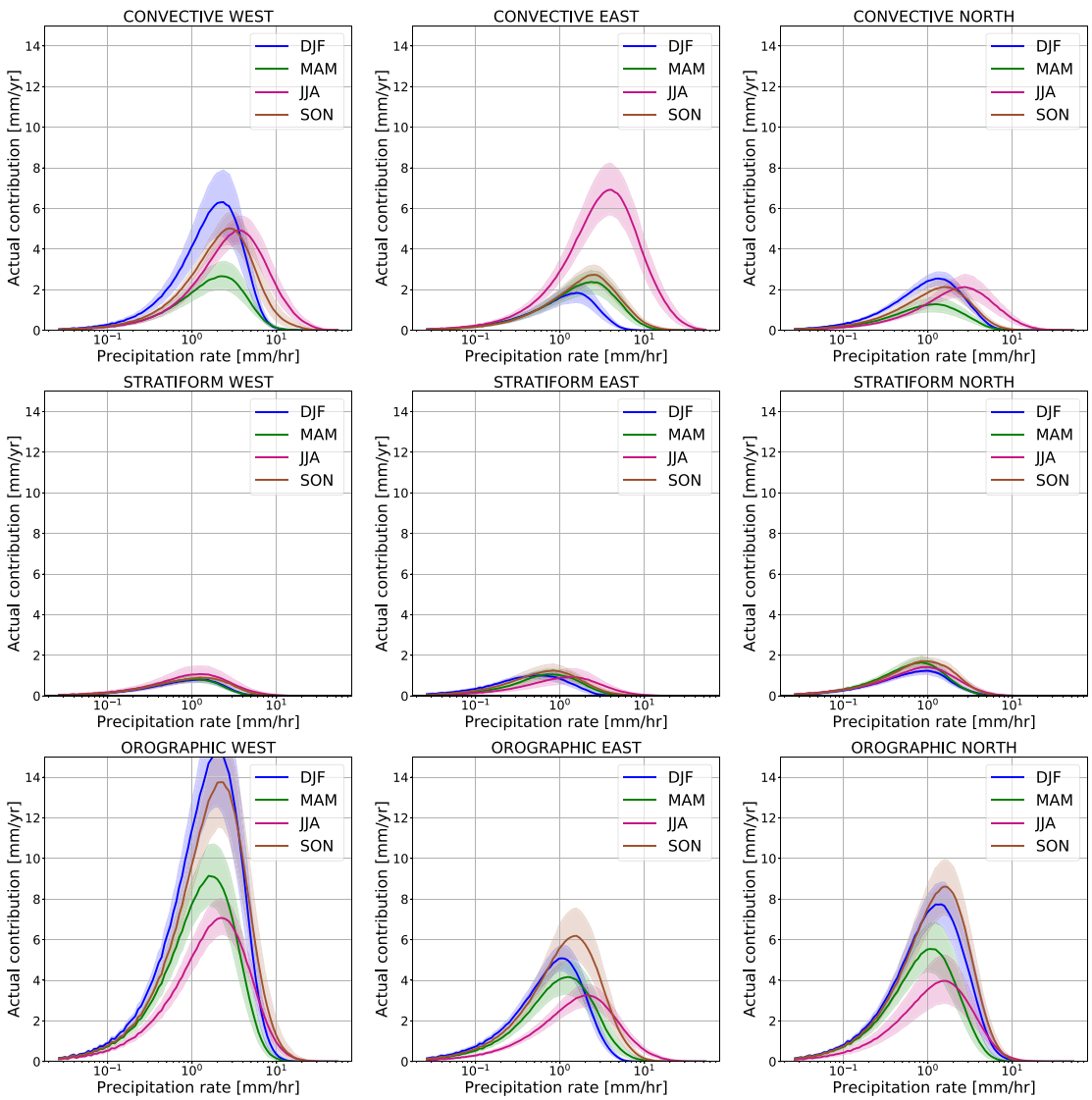

Figure E1. Same as figure 4, but for absolute historical contributions.

ORCID iDs

B Poujol https://orcid.org/0000-0002-0755-0625
P A Mooney https://orcid.org/0000-0001-5921-3105
S P Sobolowski https://orcid.org/0000-0002-6422-4535

References

Ban N, Schmidli J and Schär C 2014 Evaluation of the convection-resolving regional climate modeling approach in decade-long simulations *J. Geophys. Res. Atmos.* **119** 7889–907
Benestad R E 2018 Implications of a decrease in the precipitation area for the past and the future *Environ. Res. Lett.* **13** 044022
Berg P, Moseley C and Haerter J O 2013 Strong increase in convective precipitation in response to higher temperatures *Nat. Geosci.* **6** 181
Berthou S, Kendon E J, Chan S C, Ban N, Leutwyler D, Schär C and Fosser G 2018b Pan-European climate at convection-permitting scale: a model intercomparison study *Clim. Dyn.* **55** 35–59
Berthou S, Kendon E J, Chan S, Fosser G, Rowell D, Roberts M, Tucker S, and Stratton R 2018a Met Office Europe and Africa climate change projections at convection-permitting scale *2nd annual meeting CORDEX-FPS on convection over Europe and the Mediterranean, (Lisbon, Portugal)*
Brisson E, Van Weverberg K, Demuzere M, Devis A, Saeed S, Stengel M and van Lipzig N P 2016 How well can a convection-permitting climate model reproduce decadal statistics of precipitation, temperature and cloud characteristics? *Clim. Dyn.* **47** 3043–61
Cannon D J, Kirshbaum D J and Gray S L 2012 Under what conditions does embedded convection enhance orographic precipitation? *Q. J. R. Meteorol. Soc.* **138** 391–406
Chan S C, Kahana R, Kendon E J and Fowler H J 2018 Projected changes in extreme precipitation over Scotland and Northern England using a high-resolution regional climate model *Clim. Dyn.* **51** 3559–77
Clausius R 1850 Über die bewegende Kraft der Wärme und die Gesetze, welche sich daraus für die Wärmelehre selbst ableiten lassen *Ann. Phys., Lpz.* **155** 368–97
Coppola E *et al* 2019 A first-of-its-kind multi-model convection permitting ensemble for investigating convective phenomena over Europe and the Mediterranean *Clim. Dyn.* **55** 3–34
Dai A, Rasmussen R M, Liu C, Ikeda K and Prein A F 2017 A new mechanism for warm-season precipitation response to global warming based on convection-permitting simulations *Clim. Dyn.* **55** 343–68
de Luis M, Brunetti M, Gonzalez-Hidalgo J C, Longares L A and Martin-Vide J 2010 Changes in seasonal precipitation in the Iberian peninsula during 1946–2005 *Glob. Planet. Change* **74** 27–33
Dee D *et al* 2011 The ERA-Interim reanalysis: configuration and performance of the data assimilation system *Q. J. R. Meteorol. Soc.* **137** 533–97
Dwyer J and O'Gorman P 2017 Changing duration and spatial extent of midlatitude precipitation extremes across different climates *Geophys. Res. Lett.* **44** 5863–71
Findeisen W 1938 Die kolloidmeteorologischen Vorgänge bei der Niederschlagsbildung (Colloidal meteorological processes in the formation of precipitation). Traduction by Volken E, Giesche, A M and Brönnimann S *Meteorol. Z.* **55** 121–33
Finney D L, Marsham J H, Jackson L S, Kendon E J, Rowell D P, Boorman P M, Keane R J, Stratton R A and Senior C A 2019 Implications of improved representation of convection for the East Africa water budget using a convection-permitting model *J. Clim.* **32** 2109–29
Fischer E M and Knutti R 2016 Observed heavy precipitation increase confirms theory and early models *Nat. Clim. Change* **6** 986
Fosser G, Khodayar S and Berg P 2017 Climate change in the next 30 years: what can a convection-permitting model tell us that we did not already know? *Clim. Dyn.* **48** 1987–2003
Gentine P, Holtslag A A, D'Andrea F and Ek M 2013 Surface and atmospheric controls on the onset of moist convection over land *J. Hydrometeoro.* **14** 1443–62
Hanssen-Bauer I *et al* 2009 *Klima i Norge 2100 Bakgrunnsmateriale til NOU Klimatilplassing*
Hesterberg T C 2015 What teachers should know about the bootstrap: resampling in the undergraduate statistics curriculum *Am. Stat.* **69** 371–86
Hong S-Y, Noh Y and Dudhia J 2006 A new vertical diffusion package with an explicit treatment of entrainment processes *Mon. Weather Rev.* **134** 2318–41
Houze R A Jr 1981 Structures of atmospheric precipitation systems: a global survey *Radio Sci.* **16** 671–89
Houze R A 2012 Orographic effects on precipitating clouds *Rev. Geophys.* **50** RG1001
Iacono M J, Delamere J S, Mlawer E J, Shephard M W, Clough S A and Collins W D 2008 Radiative forcing by long-lived greenhouse gases: calculations with the AER radiative transfer models *J. Geophys. Res. Atmos.* **113** D13103
IPCC 2013 Climate change 2013: the physical science basis
Jiménez P A, Dudhia J, González-Rouco J F, Navarro J, Montávez J P and García-Bustamante E 2012 A revised scheme for the WRF surface layer formulation *Mon. Weather Rev.* **140** 898–918
Keller M, Kröner N, Fuhrer O, Lüthi D, Schmidli J, Stengel M, Stöckli R and Schär C 2018 The sensitivity of alpine summer convection to surrogate climate change: an intercomparison between convection-parameterizing and convection-resolving models *Atmos. Chem. Phys.* **18** 5253–64
Kendon E J, Ban N, Roberts N M, Fowler H J, Roberts M J, Chan S C, Evans J P, Fosser G and Wilkinson J M 2017 Do convection-permitting regional climate models improve projections of future precipitation change? *Bull. Am. Meteorol. Soc.* **98** 79–93
Kendon E J, Roberts N M, Fosser G, Martin G M, Lock A P, Murphy J M, Senior C A and Tucker S O 2020 Greater future UK winter precipitation increase in new convection-permitting scenarios *J. Clim.* **33** 7303–18
Kendon E J, Roberts N M, Fowler H J, Roberts M J, Chan S C and Senior C A 2014 Heavier summer downpours with climate change revealed by weather forecast resolution model *Nat. Clim. Change* **4** 570
Kendon E J, Stratton R A, Tucker S, Marsham J H, Berthou S, Rowell D P and Senior C A 2019 Enhanced future changes in wet and dry extremes over Africa at convection-permitting scale *Nat. Commun.* **10** 1–14
Klingaman N P, Martin G M and Moise A 2017 ASoP (v1. 0): a set of methods for analyzing scales of precipitation in general circulation models *Geosci. Model Dev.* **10** 57–83
Lenderink G, Barbero R, Loriaux J and Fowler H 2017 Super-Clausius–Clapeyron scaling of extreme hourly convective precipitation and its relation to large-scale atmospheric conditions *J. Clim.* **30** 6037–52
Lind P *et al* 2020 Benefits and added value of convection-permitting climate modeling over Fenno-Scandinavia *Clim. Dyn.* **55** 1893–912
Liu C *et al* 2017 Continental-scale convection-permitting modeling of the current and future climate of North America *Clim. Dyn.* **49** 71–95
Loriaux J M, Lenderink G and Siebesma A P 2017 Large-scale controls on extreme precipitation *J. Clim.* **30** 955–68
Lundquist J, Hughes M, Gutmann E and Kapnick S 2019 Our skill in modeling mountain rain and snow is bypassing the skill of our observational networks *Bull. Am. Meteorol. Soc.* **100** 2473–90

Lussana C, Tveito O, Dobler A and Tunheim K 2019 seNorge_2018, daily precipitation and temperature datasets over norway *Earth Syst. Sci. Data* **11** 1531–51

Manabe S and Wetherald R T 1975 The effects of doubling the CO_2 concentration on the climate of a general circulation model *J. Atmos. Sci.* **32** 3–15

Min S-K, Zhang X, Zwiers F W and Hegerl G C 2011 Human contribution to more-intense precipitation extremes *Nature* **470** 378

Molnar P, Fatichi S, Gaál L, Szolgay J and Burlando P 2015 Storm type effects on super Clausius–Clapeyron scaling of intense rainstorm properties with air temperature *Hydrol. Earth Syst. Sci.* **19** 1753

Mooney P, Sobolowski S and Lee H 2021 Designing and evaluating regional climate simulations for high latitude land use land cover change studies *Tellus* A **72** 1–17

Muller C J, O'Gorman P A and Back L E 2011 Intensification of precipitation extremes with warming in a cloud-resolving model *J. Clim.* **24** 2784–800

Niu G-Y *et al* 2011 The community noah land surface model with multiparameterization options (Noah-MP): 1. Model description and evaluation with local-scale measurements *J. Geophys. Res. Atmos.* **116** D12109

Poujol B, Sobolowski S, Mooney P and Berthou S 2020 A physically based precipitation separation algorithm for convection-permitting models over complex topography *Q. J. R. Meteorol. Soc.* **146** 748–61

Prein A F *et al* 2015 A review on regional convection-permitting climate modeling: demonstrations, prospects and challenges *Rev. Geophys.* **53** 323–61

Prein A F and Heymsfield A J 2020 Increased melting level height impacts surface precipitation phase and intensity *Nat. Clim. Change* **10** 771–6

Rulfová Z and Kyselỳ J 2013 Disaggregating convective and stratiform precipitation from station weather data *Atmos. Res.* **134** 100–15

Schär C, Frei C, Lüthi D and Davies H C 1996 Surrogate climate-change scenarios for regional climate models *Geophys. Res. Lett.* **23** 669–72

Singh M S and O'Gorman P A 2014 Influence of microphysics on the scaling of precipitation extremes with temperature *Geophys. Res. Lett.* **41** 6037–44

Skamarock W C, Klemp J B, Dudhia J, Gill D O, Barker D M, Wang W and Powers J G 2005 A description of the advanced research WRF version 2 *Technical Report* (National Center For Atmospheric Research Boulder)

Sui C-H, Li X and Yang M-J 2007 On the definition of precipitation efficiency *J. Atmos. Sci.* **64** 4506–13

Thompson G, Field P R, Rasmussen R M and Hall W D 2008 Explicit forecasts of winter precipitation using an improved bulk microphysics scheme. Part II: implementation of a new snow parameterization *Mon. Weather Rev.* **136** 5095–115

Vergara-Temprado J, Ban N, Panosetti D, Schlemmer L and Schär C 2020 Climate models permit convection at much coarser resolutions than previously considered *J. Clim.* **33** 1915–33

Westra S, Fowler H, Evans J, Alexander L, Berg P, Johnson F, Kendon E, Lenderink G and Roberts N 2014 Future changes to the intensity and frequency of short-duration extreme rainfall *Rev. Geophys.* **52** 522–55